CO_2激光作用对直流 TIG电弧温度的影响

吴世凯，　肖荣诗
（北京工业大学 激光工程研究院，北京　100124）

摘　要：在 CO_2 激光垂直穿过 TIG电弧条件下，对激光作用电弧前、后的电弧等离子体局部光谱特征进行了分析，并采用波尔兹曼图法计算了电弧局部电子温度，研究了激光对电弧等离子体轴向温度分布影响的基本规律。结果表明，激光作用电弧后，电弧等离子体的光谱特征保持不变，但整体辐射强度增加；从激光作用位置到阳极区间的电弧温度升高，而靠近阴极处的电弧温度基本保持不变；一定功率的激光束作用 TIG电弧不同位置时，其作用位置处的电弧温度基本相当，这是由于电弧等离子体仅提供初始电子，而激光束是影响相互作用后电弧温度的主要因素。

关键词：激光；电弧；光谱分析；电弧温度；逆韧致辐射吸收
中图分类号：TG456.7　　文献标识码：A　　文章编号：0253-360X(2011)02-0101-04


吴世凯

0　序　　言

由于激光焊接对被焊工件的间隙及位置精度要求很高，这大大限制了其工业应用。激光-电弧复合焊接是将两种物理性质、能量传输机制截然不同的热源复合，作用在同一熔池而形成焊缝，它充分发挥了两种焊接热源各自的优势，弥补单一热源焊接的不足[1]。近年来，激光-电弧复合焊接得到了广泛关注和积极研究[2,3]。

在激光-电弧复合焊接过程中，激光束对电弧静特性、电弧形态、能量分布等特性产生重要影响[4-6]。电弧等离子体宏观特性的变化与等离子体温度密切相关[7]。基于物质的光辐射所获取的光谱分析方法是等离子体温度诊断的主要方法之一[8,9]。胡绳荪等人[10]采用 Stark展宽光谱分析法测量了脉冲激光、TIG电弧以及激光-TIG电弧复合的电子密度。Hu等人[11]测量了 Nd:YAG-TIG复合焊接低碳钢时，电弧不同区域的电子温度及等离子体成分变化。结果表明，在激光功率 500 W，电弧电流 100 A时，由于激光辐照下材料的蒸发，电弧中 Fe离子浓度增加，而 Ar离子浓度降低。刘黎明等人[12]研究了 350 W脉冲 YAG激光与 100 A的 TIG电弧复合焊接镁合金时电弧温度及电子密度变化，结果表明，复合焊接时，电弧温度从没有激光作用的 12 000～15 600 K降低为 8 500～12 000 K，分析认为激光辐照条件下的母材蒸发对等离子体温度及电子密度有重要的影响。

为系统研究激光作用电弧后的电弧温度变化，深刻理解激光-电弧相互作用时，电弧内部的一些重要性质和物理化学过程，甄别激光-电弧相互作用的根本机制，文中采用无靶条件下，CO_2 激光垂直入射电弧的布置方式，通过对激光垂直穿过 TIG电弧等离子体后的光谱特征分析，研究了激光对电弧等离子体温度影响的基本规律。

1　试验方法

试验采用 Rofin DC035 Slab CO_2 激光器，弧焊电源为 Fronius TS5000数字焊机。试验布置如图 1所示。光束经焦距 300 mm的聚焦镜聚焦后，垂直作用于直流 TIG电弧，焦点位于电弧轴线，其中聚焦光斑直径为 0.27 mm。电弧电极为铈钨极，阴极与阳极直径分别为 2.5 mm和 30 mm，电极间距为 6 mm。电弧气氛为 Ar(15 L/min)。Molectron 3 sigma功率计放置在电弧后方，分别测量穿过电弧前、后的激光功率。同时使用 PHOTRON Fastcam 1024 R2彩色高速摄像仪(拍摄频率 f=8 000帧/s)记录电弧形态变化，使用 PI Acton Research SpectraPro 2500 瞬态光谱仪分别记录电弧不同部位的局部光谱，通过对电弧局部位置的光谱进行分析，采用波尔兹曼图法计算电弧局部温度。

收稿日期：2009-10-19
基金项目：北京市教委科技发展计划基金资助项目（KZ200710005003）

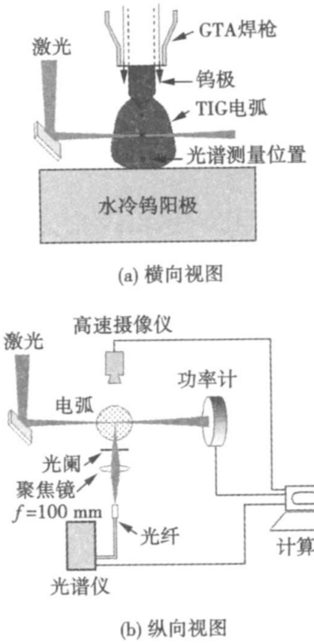

图 1 试验布置示意图
Fig. 1 Experimental setup

2 试验结果

2.1 电弧光谱特征

图 2所示为激光作用 TIG电弧前、后的电弧光谱. 由图可见, TIG电弧的光谱为在连续辐射背景上叠加的特征谱线, 其中特征谱线集中在 400 ~550 nm以及 700 ~850 nm波段, 主要为氩元素的原子谱线 Ar Ⅰ. 激光作用后, 采集的谱线形态几乎保持不变, 其特征谱线仍以 Ar Ⅰ谱线为主, 但整体辐射强度增加, 特别是在 400 ~550 nm的低频波段, 特征谱线相对强度增幅高于 700 ~850 nm波段. 随激光功率的增加, 整体辐射强度及特征谱线的相对强度增加, 但电弧中仍以一次电离为主.

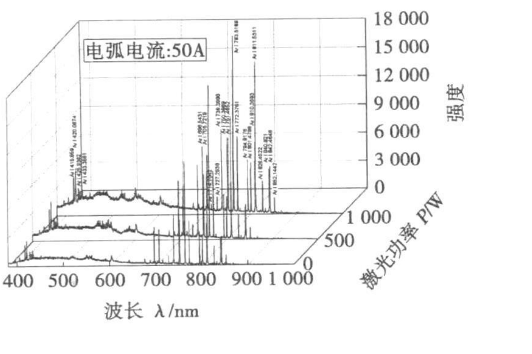

图 2 激光未作用及激光作用后的电弧光谱特征
Fig. 2 Spectral characteristics of TIG arc and TIG arc with action of CO_2 laser

2.2 电弧温度计算

基于光谱分析, 测量电弧等离子体温度的方法有绝对强度法、相对强度法、波尔兹曼图法及谱线轮廓法等, 其中波尔兹曼图法应用了较多谱线的信息, 其测量精度较高, 获得了比较广泛的应用.

在等离子体达到局部热力学平衡 (LTE)时, 处于 k能级上的粒子数密度满足波尔兹曼分布, 有如下关系, 即

$$n_k = \frac{n_0}{Z} g_k \exp\left(\frac{-E_k}{kT}\right) \tag{1}$$

式中: n_0为中性原子数密度; n_k为 k能级的粒子数密度; Z为配分函数; g_k为统计权重; E_k为高能级的电离能; k为波尔兹曼常数; T为电子温度.

由高能级 E_k向低能级 E_i跃迁时, 辐射的特征谱线强度 I_{ki}可以表示为

$$I_{ki} = A_{ki} h \nu_{ki} n_k \tag{2}$$

式中: A_{ki}为跃迁几率; ν_{ki}为辐射的特征光谱跃迁频率; h为普朗克常数.

整理式 (1), 式 (2), 并取对数可得

$$\ln\left(\frac{I_{ki}\lambda_{ki}}{A_{ki} g_k}\right) = \ln\left(\frac{n_0 hc}{Z}\right) - \frac{E_k}{kT} \tag{3}$$

式中: λ_{ki}为特征谱线波长; c为光速; $\ln(n_0 hc/Z)$为与谱线种类无关的常数, 用最小二乘法把 $\ln(I_{ki}\lambda_{ki}/A_{ki} g_k)$与 E_k拟合为一条直线, 其斜率为 $-\frac{1}{kT}$即可求得等离子体的电子温度. 利用波尔兹曼图法计算等离子体温度, 需选取多条谱线. 根据谱线选取的原则[13,14], 并对照 Ar元素原子谱线表, 选择如下 Ar Ⅰ谱线, 其原子参量见表 1[15]. 图 3所示为电弧电流为 50 A时, 计算的电弧中间位置处温度的波尔兹曼图, 计算得该位置处的电子温度为 13 094 K. 图 4所示为不同电流条件下, 电弧沿轴向的温度分布曲

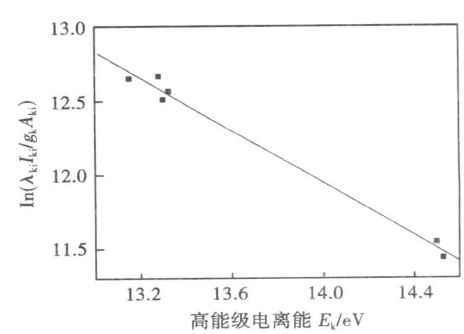

图 3 TIG电弧中心位置处的波尔兹曼图 (I=50 A)
Fig. 3 Boltzmann plot of TIG arc center (I=50 A)

表 1　Ar I特征谱线原子参量

Table 1　Atomic data of Ar I emission spectral lines

波长 λ/nm	低能级电离能 E_i/eV	高能级电离能 E_k/eV	跃迁几率 A_{ki}/(10^6·s^{-1})	统计权重 g_i	统计权重 g_k
415.859	11.548 353	14.528 912	1.4	5	5
420.067 4	11.548 353	14.499 052	0.967	5	7
696.543 1	11.548 353	13.327 856	6.39	5	3
706.721 8	11.548 353	13.302 226	3.8	5	5
714.704 2	11.548 353	13.282 638	0.625	5	3
772.376 1	11.548 353	13.153 143	5.18	5	3

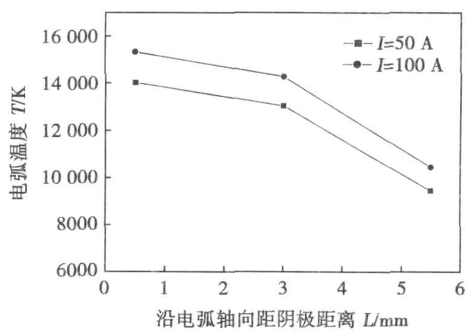

图 4　TIG电弧的轴向温度分布

Fig. 4　Arc temperature distribution along axis with different currents

线. 从图 4中可以看出, TIG电弧的温度在 10 000 ~ 15 000 K左右,从阴极区向阳极区逐渐降低,随电弧电流增加, TIG电弧不同区间的温度都有所升高.

2.3　激光对电弧温度的影响

图 5所示为 500 W激光束穿过 TIG后的电弧轴向温度分布. 从图 5中可以看出,激光作用于不同电流的 TIG电弧后,相比激光未作用时,电弧的轴向温度分布发生明显变化,其中激光作用位置到阳极区间的电弧温度升高,而阴极位置处的电弧温度基本没有变化. 当激光作用阴极区时,则整个电弧空间的温度都有所升高.

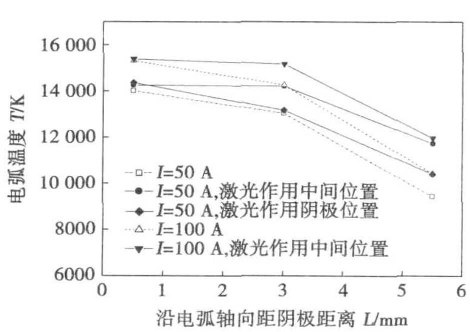

图 5　激光作用 TIG电弧后的轴向温度分布 (P=500 W)

Fig. 5　Arc temperature distribution along axis with action of laser (P=500 W)

图 6所示为激光功率 500 W,电弧电流为 50 A时,激光穿过电弧不同位置时,激光作用位置处的局部电弧温度. 从图 6中可以看出,激光作用前,电弧轴向不同位置处的温度存在很大差别,从阴极区的约 14 000 K降低到阳极区的 9 400 K左右;激光作用后,其作用位置处的电弧局部温度基本相当,都在 14 000 K左右.

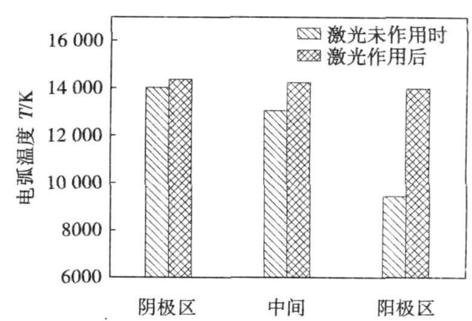

图 6　激光作用 TIG电弧不同位置的局部温度 (I=50 A, P=500 W)

Fig. 6　Local arc temperature of arc and arc with laser incident (I=50 A, P=500 W)

3　分析与讨论

激光作用电弧时,电弧等离子体将通过逆韧致辐射吸收部分激光能量,使电弧的总功率增加[4]. 在热平衡条件下,单位时间注入单位体积电弧等离子体总能量与热传导、对流及辐射散失的能量相等,因此随电弧等离子体的总功率增加,整体辐射强度增加,辐射散热增强. 由于电弧总功率随入射激光功率的增加而增加,电弧等离子体的整体辐射强度也随激光功率的增加而增加.

由于电子密度与电弧温度密切相关. 一定功率的激光束作用电弧后,电弧空间中高密度的自由电子通过逆韧致辐射吸收激光能量,使作用位置处的等离子体温度升高,导致局部电离度和导电粒子数

增加. 同时, 激光束的功率密度远高于电弧电功率密度, 对于给定电流的电弧等离子体, 在热驱动电离机制作用下, 作用位置处的电弧等离子体温度将主要由激光束决定, 而不受初始电子密度的影响, 即激光作用位置对激光作用后的电弧温度影响不大. 因此激光作用电弧不同位置时, 尽管初始的电弧局部温度存在很大差别, 但激光作用后的电弧温度基本相同, 如图 6所示. 这证实了文献 [6] 中关于平均线性吸收系数基本不受激光作用位置影响的试验结果.

根据电弧导电机制, 弧柱电流主要为电子流. 在电子流向阳极的定向运动作用下, 电弧吸收的激光能量将主要向阳极输运, 这是激光作用电弧后, 激光作用位置处到阳极区间的电弧温度升高的主要原因. 另外, 由于激光穿过电弧阴极区时, 电弧吸收的激光能量少, 所以激光作用位置到阳极区间的温度升高幅度小. 激光作用电弧中间位置及阳极区时, 电弧吸收的激光能量多, 激光作用位置处到阳极区间电弧温度大幅增加.

等离子体电子温度的计算是在 LTE的假设条件下进行的, 作为必要条件, 根据 Griem判据, 其等离子体电子密度应大于 10^{23} m^{-3}[13]. 对于上述计算的电弧温度, 在仅考虑电弧一次电离的条件下, 根据 Saha方程, 计算的电弧中的电子密度约为 1.5×10^{23} m^{-3}, 满足局部热力学平衡的假设.

4 结 论

(1) CO_2 激光作用 TIG电弧后, 电弧的光谱特征保持不变, 其特征谱线仍以 Ar I谱线为主, 电弧中仍以一次电离为主, 但整体辐射强度增加. 随激光功率的增加, 特征谱线的相对强度及整体辐射强度增加.

(2) CO_2 激光作用 TIG电弧后, 激光作用位置到阳极区间的电弧温度升高, 而阴极区的电弧温度基本没有变化.

(3) CO_2 激光作用一定电流的 TIG电弧后, 激光作用位置对作用后的局部电弧温度影响不大.

参考文献:

[1] Steen W M. Arc augmented laser processing of materials[J]. Journal of Applied Physics, 1980, 51(11): 5636－5641.

[2] Mahrie A, Beyer E. Hybrid laser beam welding-classification, characteristics, and applications[J]. Journal of Laser Applications, 2006, 18(3): 169－180.

[3] Ribic B, Palmer T A, DebRoy T. Problems and issues in laser-arc hybrid welding[J]. International Materials Reviews, 2009, 54(4): 223－244.

[4] 张寰臻, 吴世凯, 肖荣诗. CO_2 激光作用下直流 TIG电弧特性分析[J]. 焊接学报, 2009, 30(3): 97－100.
Zhang Huanzhen, Wu Shikai, Xiao Rongshi. Characteristics of DC TIG arc with the action of a vertically incident CO_2 laser beam[J]. Transactions of the China Welding Institution, 2009, 30(3): 97－100.

[5] 吴世凯, 肖荣诗, 张寰臻. 电弧气氛对 CO_2 激光与 TIG电弧相互作用的影响[J]. 焊接学报, 2009, 30(10): 81－85.
Wu Shikai, Xiao Rongshi, Zhang Huanzhen. Effect of arc atmosphere on CO_2 laser beam and TIG arc interaction[J]. Transactions of the China Welding Institution, 2009, 30(10): 81－85.

[6] 张寰臻, 吴世凯, 肖荣诗. TIG电弧对高功率 CO_2 激光光束特性的影响[J]. 焊接学报, 2009, 30(7): 29－32.
Zhang Huanzhen, Wu Shikai, Xiao Rongshi. Influence of TIG on characteristics of high power CO_2 laser beam[J]. Transactions of the China Welding Institution, 2009, 30(7): 29－32.

[7] Murphy A B. Thermal plasma in gas mixtures[J]. Journal of Physics D: Applied Physics, 2001, 34(10): R151－R173.

[8] Slade P G, Schulz-Gulde E. Spectroscopic analysis of high-current free-burning ac arcs between copper contacts in argon and air[J]. Journal of Applied Physics, 1973, 44(1): 157－162.

[9] Szymanski Z, Kurzyna J. Spectroscopic measurements of laser induced plasma during welding with CO_2 laser[J]. Journal of Applied Physics, 1994, 76(12): 7750－7756.

[10] 胡绳荪, 张绍彬, 赵家瑞. 电弧强化激光焊[J]. 焊接学报, 1993, 14(3): 159－163.
Hu Shengsun, Zhang Shaobin, Zhao Jiarui. Arc augmented laser welding[J]. Transactions of the China Welding Institution, 1993, 14(3): 159－163.

[11] Hu B, Ouden G D. Laser induced stabilization of the welding arc[J]. Science and Technology of Welding and Joining, 2005, 10(1): 76－80.

[12] Liu L M, Hao X F. Study of the effect of low-power pulse laser on arc plasma and magnesium alloy target in hybrid welding by spectral diagnosis technique[J]. Journal of Physics D: Applied Physics, 2008, 41(9): 205202.

[13] Griem H R. Plasma spectroscopy[M]. New York: McGraw－Hill, 1964.

[14] Duley W W. Laser welding[M]. New York: John Wiley & Sons, Inc, 1998.

[15] National institute of standards and technology database[DB/OL]. http://physics.nist.gov/PhysRefData/ASD/lines_form.html.

作者简介: 吴世凯, 男, 1976年出生, 博士研究生. 主要从事激光材料加工、复合焊接方面的研究工作. 发表论文 10余篇. Email: wushikai@bjut.edu.cn

Science and Technology, Nanjing University of Aeronautics and Astronautics, Nanjing 210016, China; 2. College of Mechanical Engineering, Huaiyin Institute of Technology, Huaian 223001, China; 3. Zhejiang Xinrui Welding Material Co., Ltd., Shengzhou 312000, China). p 93—96

Abstract: Cu/Al dissimilar metals were brazed with Zn-Al filler metals by torch-brazing technology, and the effects of Al on the spreadability and microstructure of Zn-Al filler metal were investigated separately. Moreover, the strength and microstructure of the brazed joint were also studied. Results indicate that the strength of the brazed joints achieves the optimum status when the Al content of filler metals is 15%. SEM and EDS are used to study the microstructure and phase constitution of the filler metals and brazed joints respectively. Experimental results show the microstructures of brazed joints are mainly consisted of Zn-based solid solution when Al content is low. However, $CuAl_2$ intermetallic compounds can form in the brazing seam region with increase of Al content. When Al content is 22 wt%, $CuAl_2$ intermetallic compounds become coarse, and the strength of brazed joint decreases.

Key words: Cu/Al; brazed joint; mechanical property; microstructure; $CuAl_2$ phase

FEM simulation of calibration on strain release coefficients in blind hole method

MA Wenbo[1,2], CHEN Shuguang, LIU Huiqiong, LIN Wen[2], SHEN Yulong, LIU Jipu[1] (1. School of Mechanical Engineering, Xiangtan University, Xiangtan 411105, China; 2. Hunan Special Equipment Inspection & Testing Center, Changsha 410000, China). p 97—100

Abstract: The significant error of the measuring result may arise when measuring welding residual stress by means of the blind hole method. Because the stress around the hole exceed the yield limit, the plastic deformation induces plastic strain. Therefore, based on the principle of the calibration experiment, the strain release coefficients A and B of the steel Q345R are determined. According to the energy parameter S, the strain release coefficient A and B can be revised by the variation formulas, by this method, the result of measuring high residual stress can be more accurate. Based on the strength theory, the strain release coefficients A and B of steel Q345R, which were numerically calculated by the finite element method (FEM), coincide well with the calibration experiment results. So the FEM determination of the strain release coefficients A and B is viable.

Key words: blind-hole method; welding residual stress; strain release coefficient; calibration experiment; finite element method

Effects of CO_2 laser beam action on temperature of TIG arc

WU Shikai, XIAO Rongshi (Institute of Laser Engineering, Beijing University of Technology, Beijing 100124, China). p 101—104

Abstract: In order to understand the effects of a vertically incident CO_2 laser beam on the tungsten-inert gas (TIG) arc characteristics, the spectra of the arc plasma with the action of a vertically incident laser beam are analyzed. The electron temperature of the arc plasma is calculated by the boltzmann plot method. The results show that the electron temperature of the arc plasma with the action of CO_2 laser beam radiation is increased between the laser acting position and anode zone. The influences of laser power, arc current and laser acted position on electron temperature are also studied. The charges in electron temperature indicate that the inverse bremsstrahlung absorption of laser energy is the dominant factor influencing the electron temperature of TIG arc plasma with the action of CO_2 laser beam.

Key words: CO_2 laser; TIG arc; spectral diagnosis; electron temperature; inverse bremsstrahlung absorption

Joint performance of duplex stainless steel 2205 by laser-MIG hybrid welding

WANG Zhiyu[1], XU Haigang, WU Weiwei, ZHANG Lijuan[2] (1. Research and Development Center, Baoshan Iron & Steel Co., Ltd., Shanghai 201900, China; 2. TWI, Cambridge CB21 6AL, UK). p 105—108

Abstract: Phase ratio in weld metal and heat affected zone of duplex stainless steel will be unbalanced and joint properties deteriorated because of fast cooling rate after welding by conventional high energy density beam, so the duplex stainless steel 2205 is welded by using laser-MIG hybrid welding method, and the microstructure, mechanical property and corrosive property of welded joint are analyzed. The results show that the phase ratio of ferrite in weld metal and heat-affected zone is controlled between 40% — 70%, the microhardness and tensile strength of the joint are higher than those of base metal, the impact toughness of weld metal, fusion line and heat-affected zone at —40 ℃ is 73, 205, 190 J/cm² respectively, and the critical pitting temperature (CPT) of weld bead is 49 ℃, near the same as that of base metal. So the good joint performance of duplex stainless steel 2205 can be obtained by laser-MIG hybrid welding.

Key words: duplex stainless steel; hybrid welding; microstructure; mechanical property; critical pitting temperature

Microstructures and corrosion-resistant performance of Al twin wire MIG welded joint

RUAN Ye[1], QIU Xiaoming, GONG Wenbiao[2], ZHAO Shihang, SUN Daqian[1] (1. School of Materials Science and Engineering, Jilin University, Changchun 130025, China; 2. School of Materials Science and Engineering, Changchun University of Technology, Changchun 130012, China). p 109—112

Abstract: Microstructures and corrosion-resistant performance of 6082-T6 Al twin wire MIG welded joint are studied by SEM and XRD technology. Experiments show that the welded seam is composed of a lot of α-Al, α-Al + Mg_2Si and a few Mg_2Si, moreover, Mg_2Si largely presents in the grain boundary. Corrosion-resistant performance is studied by measuring the potentiodynamic polarization curves and corrosion surface morphologies of twin wire MIG welded joint, and the results show that corrosion-resistant performance of the matrix is better than that of the weld seam, and precipitated Mg_2Si decreases the corrosion-resistant performance of the weld seam.

Key words: 6082-T6 Al alloy; twin wire MIG; microstructures; corrosion